2007
J. Sebag / J. Barr / A. Saha / C. Claver / V. Krabbendam
LSST CLOUD COVER MEASUREMENT FOR OBSERVATION SCHEDULING
*Revista Mexicana de Astronomía y Astrofísica, vol* 31
Universidad Nacional Autónoma de México
Distrito Federal, México
pp. 30-35

# LSST CLOUD COVER MEASUREMENT FOR OBSERVATION SCHEDULING

J. Sebag,[1] J. Barr,[1] A. Saha,[1] C. Claver,[1] and V. Krabbendam[1]

## RESUMEN

Las especificaciones científicas del Large Synoptic Survey Telescope (LSST) requieren de una operación por 10 años para realizar un reconocimiento del cielo visible en múltiples filtros con revisitas frecuentes. Durante la operación nocturna regular se utilizará un programador de observaciones para seleccionar los campos a observar con una cadencia de uno cada 30 segundos. Para maximizar la eficiencia del reconocimiento, se realizarán ajustes en tiempo real al programa de observación utilizando parámetros como la nubosidad. El LSST está evaluando la utilización de cámaras tipo all-sky —con cobertura amplia del cielo— e imágenes de satélites como información para el proceso de programación de tiempo. Cámaras tipo all-sky en el visible están en operación en la mayoría de los observatorios y se han desarrollado rutinas para cuantificar automáticamente la fotometría de las imágenes. Se realizó una comparación preliminar entre las imágenes all-sky y datos satelitales contemporáneos. La evaluación de las técnicas de detección de nubes también incluye una cámara infrarroja tipo all-sky que se espera inicie operación a mediados del 2007.

## ABSTRACT

The Large Synoptic Survey Telescope (LSST) science specifications require operating the telescope for a 10-year survey of the visible sky with frequent revisits in multiple filters. During regular night operation, an o bservatory scheduler will be used to select fields to be observed on a cadence of one every 30 seconds. To maximize the survey efficiency, real time adjustments to the observation schedule will be assessed using input parameters like cloud cover. LSST is evaluating the use of infrared and optical all-sky cameras and satellite images to inform the scheduling process. Visible all-sky cameras are in operation at several observatory sites and routines have been developed to automatically quantify photometry in the images. A preliminary comparison between these all-sky images and contemporaneous satellite data has been made. The evaluation of techniques for cloud detection also includes an infrared all-sky camera that is expected to be deployed in mid 2007.

*Key Words:* **SITE TESTING**

## 1. INTRODUCTION

The Large Synoptic Survey Telescope (LSST) is a wide-field telescope designed to image the entire visible sky repeatedly every few nights (Sweeney et al. 2006). Its 10-year mission is to perform a multi-color imaging survey of the sky to unprecedented depth and width. We currently estimate that this multi-pass survey will record 2000 exposures of each 10 square degree patch of the sky in six photometric bands (filters ugrizY, 320–1050 nm) to an accumulated depth of 27 AB magnitude. In order to achieve this goal, a fast f/1.2 telescope design based on a 3-mirror system with a large effective collecting aperture of 6.5m diameter is coupled to a unique camera with a focal plane of 3 Gpixels. Together, they provide 3.5 degree field-of-view images that can be readout in a 2 sec time to maintain a rapid cadence of two exposures per 30–40 sec visit per field.

An operation simulator was implemented to simulate the different scheduling strategies and to evaluate the cadence and sky coverage patterns using real external conditions from the site (Delgado et al. 2006). The input data to the operation simulator includes a weather model and a sky model to register and to use the atmospheric conditions for evaluating the targets. Seeing and cloud cover information are part of the weather model. During regular night operation, LSST will use an observatory scheduler based on the same principle, that will select fields to be observed in a specific filter for overall survey efficiency. One of the input parameters of the scheduler will be the cloud cover of the sky during the night.

## 2. CLOUD COVER AS INPUT FOR OBSERVATION SCHEDULING

In meteorology, clouds are usually classified in terms of appearance and location in the atmosphere. The "high clouds" classification refers to clouds at a

---

[1]National Optical Astronomical Observatory, 950 N. Cherry, Tucson AZ 85719, USA (jsebag@noao.edu).

height above 6 km and includes mainly cirrus related type of clouds. Middle clouds (2 to 6 km) and low clouds (∼2 km) are usually made of altocumulus/altostratus and stratus/stratocumulus, respectively.

In astronomy, nights are usually classified in terms of photometric hours and image quality. The "photometricity" of the night is related to the meteorological cloud cover of the sky:

- Photometric or clear time corresponds to conditions when the atmospheric extinction is minimal and stable. A minimum condition for this is the total absence of clouds.

- Spectroscopic or transparent time refers to nights which are not good enough for absolute photometry but are valuable for other observations. This is used to describe nights with high clouds like cirrus. These are usually not visible from the ground during the night and not generally distributed uniformly over the sky. In which case, the atmospheric extinction is not stable. These nights are transparent enough to get data either for spectrometry, or images where photometry can be tied to observations of the same field made during other photometric nights.

- Non-usable or opaque time is used for nights with low or middle height clouds. Due to their form, density and short distance from the ground, these are usually distinguishable by the observer against the night background. They can either affect partial areas of the sky or its totality.

Traditionally, observations are taken during photometric and spectroscopic hours. During spectroscopic nights, LSST observations will be carried out since it gathers temporal information, and because image quality can still be good. The scheduler will be able to adjust the sequence of observations based on the photometric conditions of the different areas on the sky in real time. The purpose is to maximize the efficiency of the data collection time and the efficiency of the survey mission.

LSST is evaluating the use of visible and infrared all-sky cameras and satellite images as sources of cloud cover data to inform the scheduling process. Visible all-sky cameras are in operation at several observatories. These cameras have been used in site testing campaigns. Routines have been developed to automatically quantify the photometry in the images (Sebag et al. 2006). We present here a preliminary comparison between the all-sky camera images and contemporaneous satellite data.

LSST is also testing an infrared all-sky camera that is expected to be installed in late 2007 in Chile on Cerro Pachón, near the location where the LSST telescope will be built. The camera will be located next to a visible all-sky camera in order to compare the images from both instruments. In this paper, we review the current plan for testing this system.

## 3. AUTO-PHOTOMETRY ANALYSIS OF VISIBLE ALL-SKY CAMERA IMAGES

Visible all-sky cameras built at the Cerro Tololo Inter-American Observatory (CTIO) in Chile (Walker et al. 2006), are used to acquire images automatically every night through five different bands. The camera on Cerro Pachón is called SASCA and the one on San Pedro Mártir is called MASCA. The images are accessible in real-time on their respective webservers and short movies are available to provide a qualitative assessment of cloud cover during the night. The camera system includes a Nikon f/2.8 fisheye lens that produces a 180° field of view image onto the 1K×1K CCD with an image scale of 0.18° per pixel.

The sky is imaged in the B and R bands and also in the z and Y filter. These last 2 bands are centered around 870 nm and 1000 nm respectively with a bandwidth of 100 nm. These were chosen to match the z and Y filters to be used by LSST in order to gather information on the temporal and spatial variations in extinction at these wavelengths. The fifth filter is a sodium Na filter centered at 589nm to monitor light pollution from sodium lights. The sequence of images is rapidly taken through the 5 filters with an exposure time per filter dependent on the moon's presence.

A. Saha developed an algorithm for the quantitative analysis of the images to extract the photometry of bright stars. First, the mapping from alt-az on the sky to (X,Y) coordinates on the image is derived and calibrated using the projection provided for the lens, the pixel size of the CCD, and alignment of the optical center and its orientation. The positions of the stars are computed from the local sidereal time-stamp of each image. The centroid of each star is then determined by using a 3-pixel FWHM Gaussian fit centered on the predicted position to allow for some inaccuracy in the calibration. A preliminary background (sky) is evaluated as the mean value in an annulus of 6 to 8 pixel radius (1.2 to 1.6 deg) on the sky. Using this tentative value of the sky, the aperture totals are computed for apertures of increasing radius. The variance in the aperture magnitudes for the range of apertures
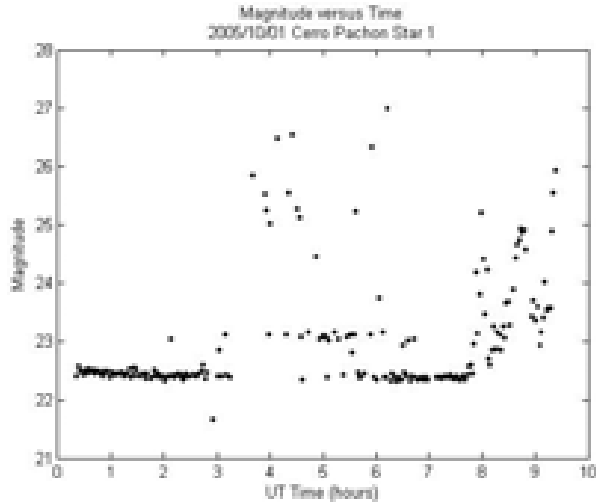
Fig. 1. Magnitude versus time for the star Alpha Eridanus (Achernar-star 1) during the night 2005-10-01 at Cerro Pachon.
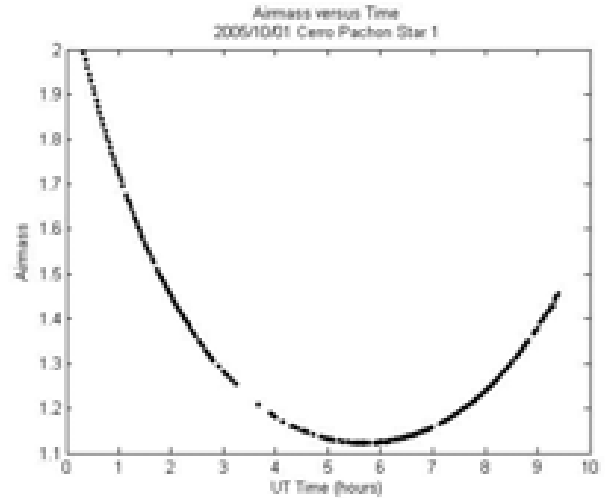


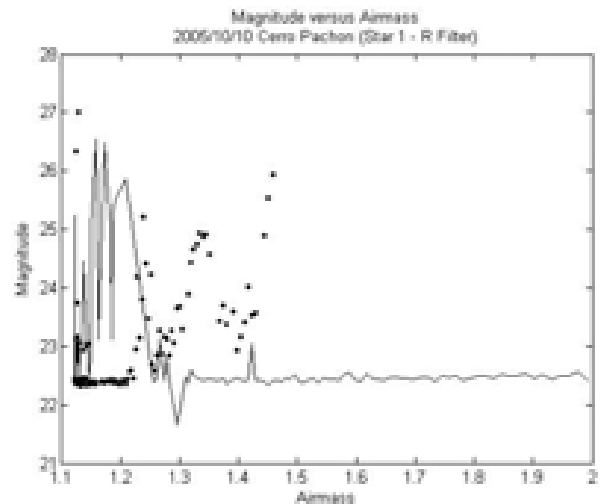Fig. 2. Airmass versus time for the same star.



Fig. 3. Magnitude versus airmass for the same star. On the plot, we used a line during the ascending part of the trajectory and dots for the descending part.

from 5 to 10 pixel radius is computed. The computation is repeated for a range of assumed values of sky (about the initial value), and the value of sky, for which the variance of aperture measurements in the 5 to 10 pixel aperture radius range is minimal, is the adopted value of the background. The reported magnitude of the star is calculated using this value for the background, and using a 5-pixel (1 degree) radius aperture. Tests on the SASCA data on a clear night show that the photometry on isolated first and second magnitude stars is repeatable with an RMS of 2–4 percent. The measuring aperture size as defined above is possibly larger than it needs to be. Making it smaller may extend the applicability to fainter and more numerous stars, but we are first analyzing data in that configuration. The photometry procedure is currently applied to all the images in the R band with no moon.

For each star, a magnitude versus time plot per filter is generated each night followed by a magnitude versus airmass plot. An example is given in Figures 1 to 3 for one of the measured stars during the night of Oct. 10 2005. In addition, Figure 2 shows the variations of the airmass versus time for that same star. A linear fit is done on the former curves and the zero term and the extinction are estimated. The RMS of the fit is also calculated for each star. We have found that, with this process, the measured magnitudes on the stars scatter with respect to their catalog values in the same bandpass, but the measured magnitudes are repeatable to a few percent within the all-sky camera measurements on clear nights. A sky bright-

ness of 22 mag sq. arcsec−1, adds up to 2.2 mags in the 1 degree radius aperture. While this value is indeed subtracted, it is easy to see that such subtraction is heavily affected by variations in object contamination. Thus, what we are really measuring is the total sum of what lies within the measuring aperture, relative to its surroundings. This explains the lack of agreement against the catalog magnitudes of the stars, while also explaining why the all-sky camera magnitudes are repeatable.

For the purpose of the comparison, a zero term reference per star was established by computing a histogram of all the analyzed nights. That zero term
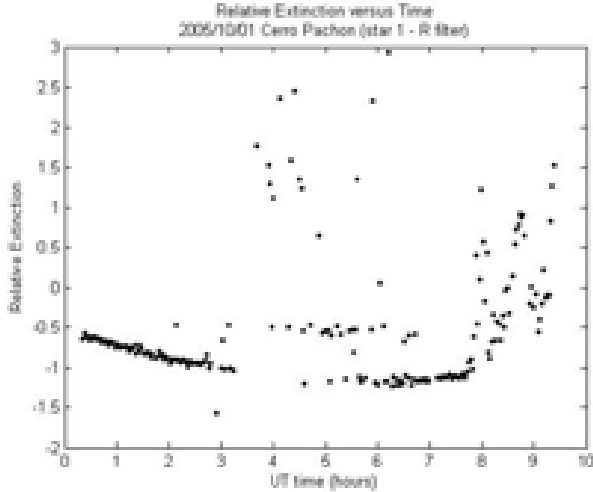
Fig. 4. Relative Extinction versus time for the night 2005-10-01 at Cerro Pachon along the trajectory of the star Alpha Eridanus (star 1).
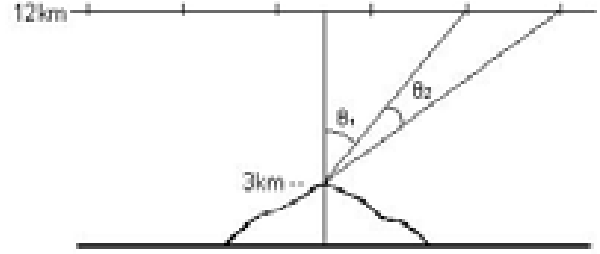


Fig. 5. Schematic diagram showing the 3×3 and 5×5 cross section above the site. The observed area corresponds approximately to 40° and 54° zenith angles at the Tropopause level.

reference is a fixed value per star. Then, an instantaneous non-normalized relative extinction is estimated for each image by subtracting this reference from the measured magnitude and by dividing by the airmass at the time of the measurement . An example of this relative extinction versus time is shown in Figure 4.

## 4. COMPARISON WITH SATELLITE DATA

After the implementation of the algorithm, a comparison of the photometry analysis with satellite data was started in order to verify the general correlation of our measurements with a totally different set of data. Satellite observations have the advantage of covering a wide field of view with a spatial resolution suitable for such a comparison. The satellite-derived cloud cover data analysis was performed by D. A. Erasmus. The general methodology of satellite cloud cover analysis employed was that developed, revised and applied in earlier studies for GOES8 data (Erasmus et al. 2002). At $6.7 \mu m$, under clear conditions emission reaches the satellite from water vapor in the middle and upper troposphere. The brightness temperature may be calibrated in terms of the relative humidity of that layer and is referred to as the Upper Tropospheric Humidity (UTH). If the UTH exceeds specified values, the presence and thickness of high altitude (9–12 km) cirrus clouds is indicated.

The data analyzed cover the year 2005 and is from the GOES12 satellite which replaced the GOES8 satellite in April 2003. It usually provides coverage between 1 and 3 times per hour. Compared to GOES8, the GOES12 IR window channel

at 10.7 $\mu m$ is the same. However, the water vapor channel at 6.5 $\mu m$ for GOES12 is different from the 6.7 $\mu m$ channel for GOES8. This change affects the weighting function and therefore the peak height and height range of the emitting layer. Also the spectral response function is significantly wider for GOES12. As a result, D. A. Erasmus had to perform an initial UTH calibration for GOES12 data using Soden and Bretherton's method (Soden et al. 1993, 1996) to obtain monthly calibration coefficients, because the previous calibration done for GOES8 is not applicable for GOES12 data. The accuracy of this initial calibration is limited due to the reduced quantity of data available. His plan was to repeat the calibration after having analyzed more years of images.

For the image analysis, the satellite images were divided into a 3×3 and a 5×5 pixel grid which corresponds approximately to an area of observation within 40° and 54° zenith angles (cf. Figure 5). The UTH is computed for each pixel on each image. This value, which varies between 0 and 100%, is directly compared to the photometry analysis.

The purpose of the comparison is to verify that both sets of measurements are correlated. The comparison method consists of matching the UTH data with the photometry data using spatial and temporal information. As the stars cross the sky, they move from one UTH pixel to another. A first result of the comparison is presented in Figure 6 as an example. This work is still on-going and final results are not ready yet. This is the same plot showed in Figure 1 with an additional curve showing the recorded UTH variations during the same night. The initial comparison shows a good correlation when both data are available simultaneously. There are no UTH points between 3 and 6 h UT because no satellite data was available at that time. For GOES8 data, the threshold between clear and transparent conditions was set at a UTH of 50%. However, due to the differences

TABLE 1

ASIVA MAIN CHARACTERISTICS

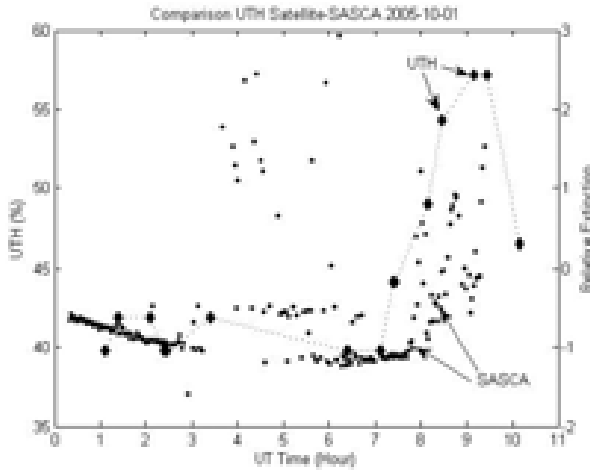| Parameter | Value | Performance Impact |
|---|---|---|
| Detector | $320 \times 240$ | pixels of ferroelectric sensor |
| Bandpass | $8 - 12 \ \mu m$ | water vapor atmospheric window |
| Pixel Size | $50 \ \mu m$ | total detector area of 16 mm $\times$ 12 mm |
| Lens F ratio | 1.4 | fisheye lens with hard protective coating |
| Filters | 5 positions | 4 filters currently installed |

Fig. 6. Comparison of Relative Extinction and UTH for the night 2005-10-01 at Cerro Pachon along the trajectory of the star Alpha Eridanus (star 1).

mentioned above, this threshold is not applicable to GOES12 data.

In the future, we are also planning to use the MASS data (Multi Aperture Scintillation Sensor) to perform a similar type of comparison (Tokovinin et al. 2003). The MASS records the variations of the flux of the acquired star in each of the annular aperture. This signal is sensitive to the presence of clouds and should be usable to perform correlations with the photometry data. Then, once these comparisons have been performed, aperture photometry will be used to generate, in real-time, relative optical transmission maps per field.

## 5. IR ALL-SKY CAMERA

In addition to the visible all sky camera , LSST has recently acquired an InfraRed All-sky Camera to be deployed in Chile on Cerro Pachon later this year. It is currently located in Tucson for testing and calibration. Such wide field-of-view systems have been developed in the past for cloud de-

tection using either a scanning device (Hull et al. 1994) or a reflective telescope (Mallama et al. 2002; APO http://irsc.apo.nmsu.edu; Suganuma et al. 2007). This system, known as ASIVA for All-Sky Infrared Visible Analyzer, uses a specially designed 180° cone angle lens (see Table 1 for main characteristics). It makes the overall system relatively compact even with the additional small all-sky visible camera installed in the same enclosure. It is designed to withstand difficult mountain-top conditions and to acquire data in an automatic manner. The unit takes a sequence of images automatically through the four filters currently installed in the camera. The images are saved in a fits format on a linux-based computer and are also displayed in real-time.

The $8 - 12 \ \mu m$ detectors are well suited for cloud detection as a cloudless atmosphere is relatively transparent at these wavelengths. If clouds are present they will be detected as warmer than the clear sky. Low and middle height altitude clouds have a temperature that approaches the surface air temperature and they usually present a high contrast with the clear sky. High cirrus clouds are colder and therefore presents a smaller contrast with the clear sky which make them more difficult to detect. Because these clouds are also thinner, their impact on the photometry needs to be assessed to estimate the detection level of the IR system. To address this issue, the plan is to compare the measurements from SASCA with ASIVA by installing them next to each other over a long period. This will allow us to acquire data in different cloud cover conditions in order to correlate temporal and spatial variations simultaneously.

The four filters included in ASIVA provide also the unique capability of measuring the cloud's emission in different wavebands (Table 2). These are located in front of the camera in a filter wheel. Recent studies in remote sensing (Yang et al. 2005) have shown that slope and y-intercept information computed from enveloping profiles at different wave-

TABLE 2

ASIVA INFRARED FILTERS

| Center (micron) | Bandpass ($\mu$m) |
|---|---|
| 8 | 7.6 to 8.3 |
| 10.5 | 10 to 11 |
| 12 | 11.4 to 12.5 |
| 10 | 8 to 12 |

lengths could provide information on the effective size and optical thickness of cirrus clouds. In a similar way, ratios of the signal between the different filters could offer some information on the clouds characteristics and could provide a quantitative method to reconstruct the optical transmission map.

### 6. CONCLUSION

This is still a work in progress. The visible all-sky camera data analysis photometry software is in testing phase and comparison with other methods of cloud detection will continue to be investigated. The IR all-sky camera offers a new alternative for cloud detection that will complement this effort.

### REFERENCES

Delgado, F., Cook, K., Miller, M., Allsman, R., & Pierfederici, F. 2006, Proc. SPIE, 6270, 62701D
Erasmus, D. A., & Sarazin, M. 2002, ASP Conf. Proc. 266, Astronomical Site Evaluation in the Visible and Radio Range, ed. J. Vernin, Z. Benkhaldoun, & C. Muñoz-Tuñón (San Francisco: ASP), 310
Hull, C. L., Limmongkol, S., & Siegmund, W. A. 1994, Proc. SPIE, 2199, 852
Mallama, A., & Degan, J. J. 2002, PASP, 114, 913
Sebag, J., Krabbendam, V., Claver, C., Barr, J., Barr, J., Kantor, J., Saha, A., & Erasmus, D. A. 2006, Proc. SPIE, 6267, 62671R
Soden, B. J., & Bretheton, F. P. 1993, J. Geophys. Res. 96, 16669
————. 1996, J. Geophys. Res., 101, 9333
Suganuma, M., et al. 2007, PASP, 119, 567
Sweeney, D., & the LSST collaboration 2006, Proc. SPIE, 6267, 626706
Takato, N., Okada, N., Kosugi, G., Suganuma, M., Miyashita, A., & Uraguchi, F. 2003, Proc. SPIE, 4837, 872
Tokovinin, A., Kornilov, V., Shatsky, N., & Voziakova O. 2003, MNRAS, 340, 52
Walker, D., Schwarz, H. E., & Bustos, E. 2006, Proc. SPIE, 6267, 62672O
Yang, P., Tsay, S., Wei, H., Guo, G., & Ji, Q. 2005, IEEE Geosci. Remote Sens. Letters, 2, 128